Universiteit
Leiden
The Netherlands

Targeting for success: mechanistic insights into microRNA-based gene therapy for Huntington disease

Sogorb Gonzalez, M.

Citation
Sogorb Gonzalez, M. (2023, February 9). *Targeting for success: mechanistic insights into microRNA-based gene therapy for Huntington disease*. Retrieved from https://hdl.handle.net/1887/3515739

Version:	Publisher's Version
License:	Licence agreement concerning inclusion of doctoral thesis in the Institutional Repository of the University of Leiden
Downloaded from:	https://hdl.handle.net/1887/3515739

Note: To cite this publication please use the final published version (if applicable).

Chapter 3

Widespread and Sustained Target Engagement in Huntington Disease Minipigs upon Intrastriatal MicroRNA-Based Gene Therapy

Astrid Vallès[1†*], Melvin M. Evers[1†*], Anouk Stam[1], **Marina Sogorb-Gonzalez**[1], Cynthia Brouwers[1], Carlos Vendrell-Tornero[1], Seyda Acar-Broekmans[1], Lieke Paerels[1], Jiri Klima[3], Bozena Bohuslavova[3], Roberta Pintauro[2], Valentina Fodale[2], Alberto Bresciani[2], Roman Liscak[4], Dusan Urgosik[4], Zdenek Starek[5], Michal Crha[6], Bas Blits[1], Harald Petry[1], Zdenka Ellederova[3], Jan Motlik[3], Sander van Deventer[1] and Pavlina Konstantinova[1]

[1]Department of Research & Development, uniQure B.V.,Amsterdam, The Netherlands
[2]Department of Translational Biology, IRBM, Pomezia, Italy
[3]Institute of Animal Physiology and Genetics, Libechov, Czech Republic
[4]Department of Stereotactic Radioneurosurgery, Prague, Czech Republic
[5]Interventional Cardiac Electrophysiology, Brno, Czech Republic
[6]Small Animal Clinic, Veterinary and Pharmaceutical University, Brno, Czech Republic

† These authors contributed equally

Science Translational Medicine (2021); 13(588).

Abstract

Huntingtin (HTT)-lowering therapies hold promise to slow-down neurodegeneration in Huntington disease (HD). Here, we assessed the translatability and long-term durability of recombinant adeno-associated viral vector serotype 5 expressing a microRNA targeting human HTT (rAAV5-miHTT) administered by magnetic resonance imaging (MRI)-guided convention-enhanced delivery (CED) in transgenic HD (tgHD) minipigs. rAAV5-miHTT (1.2×10^{13} gc/brain) was successfully administered into the striatum (bilaterally in caudate and putamen), using age-matched untreated animals as controls. Widespread brain biodistribution of vector DNA was observed, with the highest concentration in target (striatal) regions, thalamus and cortical regions. Vector DNA presence and transgene expression were similar at 6- and 12-months post-administration. Expression of miHTT strongly correlated with vector DNA, with a corresponding reduction of mutant HTT (mHTT) protein of more than 75% in injected areas, and 30-50% lowering in distal regions. Translational pharmacokinetic and pharmacodynamic measures in cerebrospinal fluid (CSF) were largely in line with the effects observed in the brain. CSF miHTT expression was detected up to 12 months, with CSF mHTT protein lowering of 25-30% at 6- and 12-months post-dosing. This study demonstrates widespread biodistribution, strong and durable efficiency of rAAV5-miHTT in disease-relevant regions in a large brain, and the potential of using CSF analysis to determine vector expression and efficacy in the clinic.

Introduction

Huntington Disease (HD) is a devastating autosomal dominant neurodegenerative disorder caused by an extended CAG repeat in exon 1 of the huntingtin (HTT) gene, with progressive development of psychiatric, motor and cognitive symptoms (1). Neuropathology in HD precedes disease (motor) onset, especially in striatal regions, and extends throughout the brain with disease progression (2). At present, only symptomatic treatments are available, which do not address the primary pathology nor slow-down disease progression (3). Because of this high unmet need, efforts have been made to develop disease-modifying approaches for HD, many of these in clinical development or entering soon (4). HTT-lowering therapies are of particular interest, as they are conceived to knock-down the expression of the disease causative gene (5). Most of these therapies in clinical development for HD are based on the use of antisense oligonucleotides (ASOs), targeting specific regions of the HTT transcript, thereby reducing HTT mRNA and protein expression (6). Typically, ASOs are administered intrathecally on a periodical basis to ensure steady-state concentrations of the therapeutic agent (7). Based on pre-clinical studies, the expectations are that intrathecally administered ASOs efficiently reach the spinal cord and superficial brain regions (cortex), and less efficiently penetrate into deep brain regions such as caudate nucleus, unless higher doses are used (8). Nonetheless, results on cerebrospinal fluid (CSF) biomarkers show promise for HTT lowering ASOs (7), for which different trials are ongoing (ClinicalTrials.gov identifiers: NCT03761849, NCT03225833, NCT03225846). A recent study with divalent siRNAs injected into the CSF, showed sustained HTT lowering throughout the brain, holding promise for less repetitive injections and wider biodistribution of therapeutic agents (9).

In contrast to ASOs and siRNAs, adeno-associated viral vector (AAV) gene therapies for HD can be administered locally into the brain region of interest, after which they expand to interconnected regions through retrograde and anterograde transport, depending on the AAV serotype used (10). A single administration is presumed to be sufficient to ensure long-term persistence of the therapeutic transgene, especially in non-dividing cells such as neurons (11, 12). Local administration of rAAV5 was shown to result in preferential neuronal (both NeuN+ and DARPP32+) and astrocytic transduction (13, 14). AAV-based HTT-lowering therapies are in pre-clinical phases (15-19) or entering clinical development in the case of rAAV5-miHTT (ClinicalTrials.gov identifier: NCT04120493). rAAV5-miHTT is a recombinant AAV-based gene therapy expressing an engineered microRNA specifically designed to bind to HTT exon 1 (20), resulting in lowering of both wild type and mutant HTT mRNA. This approach has demonstrated efficacy and safety in in vitro models as well as in small and large animal studies, without off-target effects (20-25), supporting transition to clinical investigation. To ensure precise administration and spread of the AAV, a thorough

evaluation of the surgical approach envisaged for the clinic, in relation to the resulting biodistribution and long-term persistence in a large brain is of crucial importance. In addition, adequate translational measures to evaluate the safety, efficacy and durability of rAAV-mediated HTT lowering in patients are much needed. Efficacy and durability aspects were addressed in the present study, using minipigs as a model.

Minipigs have a good similarity to humans in terms of brain structure, cerebral blood supply and immune responses (26) and we have previously reported in the utility of tgHD minipigs to evaluate different routes of administration of rAAV5-miHTT (23). This large animal model of HD expresses a transgene encoding the first 548 amino acids of HTT with 124 glutamines under the control of the human HTT promoter (27), with relatively slow and mild phenotype development shown so far (28-32), making this model suitable for translational purposes. In the current study we have applied clinically translatable MRI-guided convention-enhanced delivery (CED) of rAAV5-miHTT in the tgHD minipig model and assessed long-term rAAV5-miHTT vector biodistribution, target engagement and HD biofluid biomarkers. The caudate nucleus and putamen were chosen as surgical target regions, as the primary affected regions in HD and with relevant connections to cortical areas, which are affected later in the disease (2). For longitudinal evaluation of biomarkers in cerebrospinal fluid (CSF), mutant (m)HTT and neurofilament light chain (NFL) were chosen as disease-specific measures as both increase with disease progression in humans (33), and miHTT as a measure for rAAV5-miHTT expression.

We here report on the feasibility, precision and efficacy of MRI-guided CED of rAAV5-miHTT in caudate and putamen of tgHD minipigs, leading to strong, sustained and brain-widespread vector distribution, human HTT protein lowering and associated biomarker changes. These results support the translational value of these measures and the continuation of rAAV5-miHTT into the clinic as promising HD-modifying agent.

Results

Successful dosing and target acquisition in caudate and putamen of tgHD minipigs using MRI-guided convention-enhanced delivery

rAAV5-miHTT encodes an engineered miRNA embedded into the human miR-415a precursor, targeting exon1 of human HTT (5' of the CAG expansion repeat) (Supplementary Figure 1A). Upon transduction, episomal expression of rAAV5-miHTT should ensure continued supply of miHTT, leading to HTT protein lowering (Supplementary Figure 1B). For HTT lowering approaches to be successful in patients, especially for gene therapy approaches where a single administration should be sufficient, it is crucial to obtain information on long-term efficacy and brain biodistribution after a single administration in a large brain. To this end, the tgHD minipig model of HD was chosen, using the same target structures and surgical approach as envisaged for the clinic. Young (4- to 6-month old, when sinus formation is not yet developing) tgHD minipigs were used. Naïve (untreated) age-matched tgHD animals were used as controls.

To increase translatability of our study, we applied an administration protocol as close as possible to the one envisaged for the clinic. Intracranial MRI-guided convection-enhanced delivery (CED) was used to administer rAAV5-miHTT in the caudate and putamen of tgHD minipigs. This is the first time that this surgical protocol for gene therapy delivery is used in this model. All sixteen tgHD minipigs used in the surgical part of the study were successfully infused into the putamen and nucleus caudate. The two striatal structures were chosen as they are key to the pathology of HD and have relevant connections to cortical regions impacted at later disease stages (2). Surgical planning was undertaken using the Renishaw neuroinspire software. Each subject was implanted bilaterally with a total of four catheters – one in each putamen and each caudate nucleus, receiving 100µl of 3x1013 gc/mL rAAV5-miHTT per catheter using the Renishaw neuroinspire planning software and drug delivery system. Gadoteriol (ProHance, 2mM) was used as a contrast agent to visualize the filling of the target structures (**Figure 1**). To confirm target acquisition, a final MR image was taken, and guiding tubes and catheters were removed ten minutes after infusion. A summary of the target acquisition is presented in **Table 1**. In general, the accuracy of the preplanning and subsequent administration was high, with a total of 60 out of 64 catheters correctly placed. The target structures (nucleus caudate and putamen) were effectively reached and correctly infused as evaluated by the target region fill with the contrast agent. The 4 unsuccessful injections (out of 64 total injections) were due to minor reflux in two cases (left putamen of animals T38 and T41), a broken Luer connection in one case (right putamen of animal T31) and a high in-line pressure due to a suture that had tied up the tubing in the last case (left caudate of animal T70). No safety issues related to the surgical

approach were observed in any of the animals throughout the experimental period, as evaluated by daily general observation, weekly body weight, and blood hematology parameters (Supplemental File S1). One TgHD minipig was sacrificed one-month post injection due to complications during CSF collection, not related to administration procedure or drug product. Hence, we demonstrate the feasibility of the MRI-guided CED surgical approach for therapeutic delivery in tgHD minipigs, with a high rate of precision of both target acquisition and structure fill in caudate and putamen.

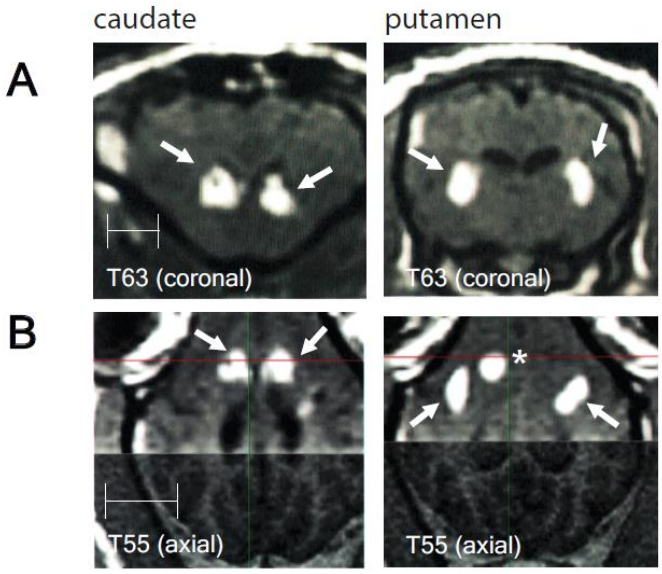

Figure 1. **Surgical delivery of rAAV5-miHTT to caudate and putamen in tgHD minipigs.** Representative coronal and axial images are shown, as well as target structure fill indicated with arrows. **(A)** Coronal view of bilateral injections in caudate (left) and putamen (right) in animal T63. **(B)** Axial view of bilateral injections in caudate (left) and putamen (right) in animal T55; part of the fill of the caudate can also be observed (indicated by *). Scale bar: 1 cm.

Table 1. Summary of target acquisition in TgHD minipigs

Subject ID	Weight (kg)	Sex	Left		Right	
			Putamen	Caudate	Putamen	Caudate
T29	30	F	OK	OK	OK	OK[#]
T41	32	M	Minor reflux	OK[#]	OK	OK
T39	32	M	OK	OK	OK	OK[#]
T45	25	F	OK	OK	OK	OK
T31	25	F	OK	OK	Failed	OK
T51	25	F	OK	OK	OK	OK
T55	15	F	OK	OK	OK	OK
T62	12	F	OK[#]	OK	OK	OK
T34	35	M	OK[#]	OK[#]	OK	OK[#]
T38	25	F	Minor reflux	OK	OK	OK
T58	22	F	OK	OK	OK	OK
T63	12	F	OK	OK	OK[#]	OK
T70	36	F	OK[#]	Failed	OK	OK
T73	36	F	OK[#]	OK	OK	OK
T87	17	M	OK	OK	OK[#]	OK
T93	17	F	OK	OK	OK	OK[#]

[#] Test material formulation distribution outside the injected structure

Widespread vector DNA distribution in the tgHD minipig brain, comparable at 6- and 12-months post-administration of rAAV5-miHTT

To evaluate the biodistribution and long-term durability of rAAV5-miHTT in the tgHD minipig brain after MRI-guided CED, different interim sacrifices were planned at 6 months and 12 months. At 6 months, three animals were sacrificed, the brains were dissected and a total of n=27 brain tissue punches were analyzed per animal, whereas of four animals n=85 punches per animal were analyzed at 12 months (Supplementary Figure 2). Brain punches were subdivided for assessment of transduction (DNA isolation), transgene expression (RNA isolation) and target engagement (protein analysis). Vector transduction was observed throughout the brain of rAAV5-miHTT injected animals, both at 6- and 12-months post-injection, with peak concentrations in target regions (caudate, putamen), limbic areas (amygdala), cortical regions, and thalamus (**Figure 2A**, Supplementary Figure 3). The highest concentrations ranged between 10^6-10^7 vector genome (VG) copies/µg DNA,

whereas the lowest concentrations, observed in pons and cerebellum, were generally just above the lower limit of quantification (LLoQ; $5x10^3$ VG copies/µg DNA). Relatively high concentrations (with respect to the LLoQ) were observed in white matter regions (in the range of 10^5 VG copies/µg DNA). Vector DNA concentrations in the different brain regions were highly comparable at 6- and 12 months post-administration, indicating sustained rAAV5-miHTT vector persistence. In spinal cord, vector DNA concentrations were mostly below LLoQ (**Figure 2B**).

Because of the importance of reaching not only target regions (caudate nucleus, putamen) but also other regions that show neurodegeneration at later stages of the disease, such as cerebral cortex, we performed a more extensive analysis of cortical vector transduction at 12 months (**Figure 2C**). The highest transduction was observed in cortical regions closer to the target areas, such as the insular and perirhinal/retrosplenial cortices (on average 10^6 VG copies/µg DNA), followed by somatomotor, and temporal cortices (>10^5 VG copies/µg DNA), and visual, cingulate, somatosensory, prefrontal and motor cortices (>10^4 VG copies/µg DNA).

With this extensive analysis of vector DNA distribution across the whole brain, we show that a one-time local injection of rAAV5-miHTT in caudate and putamen in a large HD animal model leads to strong and persistent transduction of and beyond target areas, covering all key brain regions that are affected at the different stages of HD.

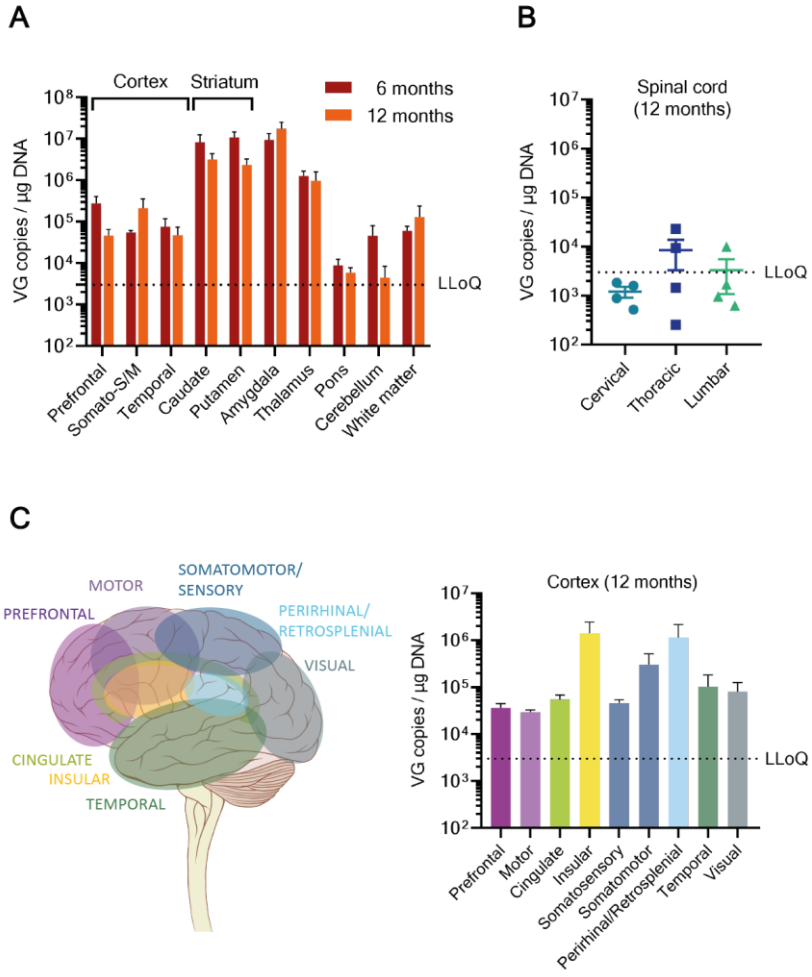

Figure 2. Vector transduction in different brain and spinal cord regions of rAAV5-miHTT injected animals. (A) Transduction in different brain areas at 6 (blue bars) and 12 (red bars) months post-injection were determined by QPCR and indicated in vector genome (VG) copies per µg of genomic DNA. **(B)** Transduction in cervical, thoracic and lumbar regions of the spinal cord at 12 months post-injection (n=4 animals/group). **(C)** Detailed view of transduction in cortical subregions 12 months post-rAAV5-miHTT. The cortical regions are color-coded in the drawing, and corresponding concentrations(in VG/µg genomic DNA) are displayed in the bar graph. *Bars represent average ± SEM; LLoQ: lower limit of quantification.*

High precision processing and therapeutic miRNA expression at 1-year post rAAV5-miHTT administration

Next to vector DNA biodistribution, expression of the therapeutic microRNA was determined. Quantification of mature mi*HTT* was performed at 12 months, in the same brain regions as for vector DNA. In line with the observed transduction pattern, mature mi*HTT* RNA molecules were detected in all analyzed brain areas from animals treated with rAAV5-miHTT, except for a small number of individual samples (<10 of approximately 170) in which miHTT expression was at or below the LLoQ (**Figure 3A**). Because the mi*HTT* detection method is specific for the active mature guide strand, its sustained expression validates the correct mechanism of action of rAAV5-miHTT from AAV cell entry, nuclear import, primary mi*HTT* expression to accurate processing. Accordingly, a highly significant correlation of mi*HTT* expression with vector DNA concentration was observed (Pearson r 0.8963, p<0.0001) (**Figure 3B**).

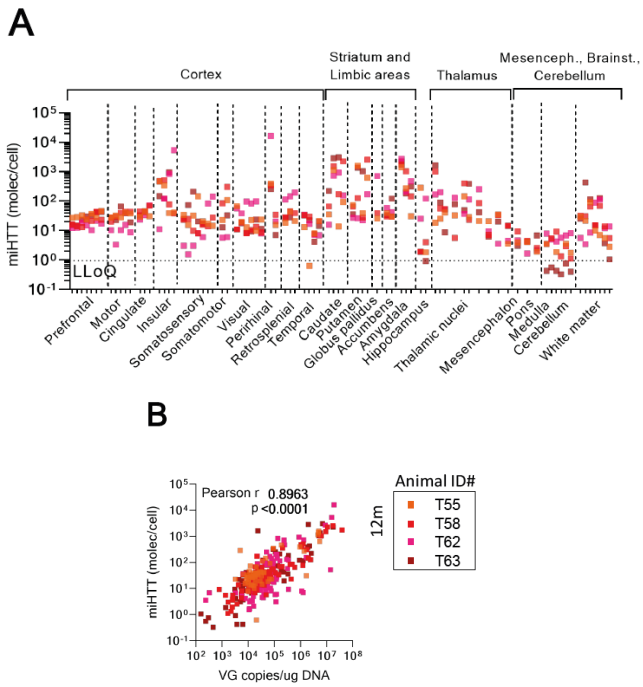

Figure 3. Brain-wide expression of mature miHTT at 12 months post-rAAV5-miHTT administration generally correlates with vector DNA concentration. (A) Mature miHTT concentrations in brain regions were determined using a specific Taqman RT- QPCR assay. Shown are the results for n=4 animals (T55, T58, T62 and T63, individually color-coded), per brain region (each dot represents the average results of one punch). *LLoQ: lower limit of quantification.*

Strong and widespread mHTT protein lowering after one-time rAAV5-miHTT administration into the caudate and putamen

To evaluate the effect of mi*HTT* on human mHTT protein lowering, all brain regions, at 6 and 12 months, were analyzed using the same method used to quantify human mHTT in CSF of patients with HD (*34, 35*). Sustained mHTT protein lowering was observed in most areas of the brain (**Figure 4A**), at 6 and 12 months after rAAV5-miHTT MRI-guided CED (**Figure 4B**). The analysis at 12 months post-rAAV5-miHTT administration, with the more extensive brain sampling, demonstrated sustained lowering of mHTT protein in all brain areas measured, except in the cerebellum. The most pronounced mHTT protein lowering was observed in putamen (average 84% lowering; 95%CI [65-104]), caudate (average 79% lowering; 95%CI [65-94]) and amygdala (average 78% lowering; 95%CI [44-112]), followed by thalamus (average 56% lowering; 95%CI [44-68]) and prefrontal cortex (average 44% lowering; 95%CI [37-51]). Although still significant, a less pronounced mHTT protein lowering was obtained in pons ($p<0.05$) and white matter regions ($p<0.005$), in line with vector DNA and mi*HTT* expression. In the somatosensory-, somatomotor- and visual-cortex, mHTT lowering did not reach statistical significance ($0.05<p<0.1$). We observed a significant global correlation between mHTT protein lowering (in % from control) and mi*HTT* expression in brain (Supplementary Figure 4, Pearson r -0.2957, $p<0.0001$). The analysis of mi*HTT* and mHTT protein concentration in tgHD minipigs supports the potential of an exceptionally widespread and pronounced effect of rAAV5-mi*HTT* therapy to lower mHTT extensively across a large brain.

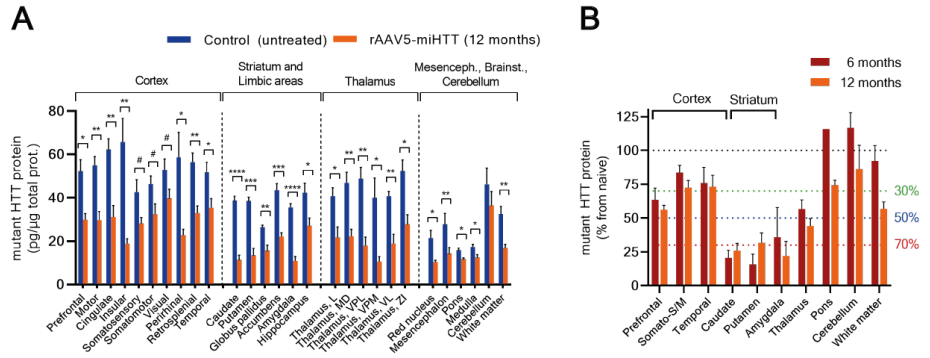

Figure 4. Sustained mHTT protein lowering across the entire tgHD minipig brain. (A) mHTT protein concentrations were determined in several brain areas, in control (untreated) and rAAV5-miHTT treated animals at 12 months post-injection. **(B)** mHTT protein lowering at 6 (blue bars) and 12 (red bars) months post injection. *Bars represent average ± SEM; statistics: two-tailed t-test, corrected p #<0.1, *<0.05, **<0.005, ***<0.0005, ****<0.0001.*

Successful detection of miHTT in cerebrospinal fluid up to one year after one-time intracranial administration allows translational monitoring of the therapeutic agent

As clinical translatable efficacy markers are notoriously challenging in central nervous system (CNS) disorders, due to the inaccessibility to the brain, the use of large (disease-modeling) animals are key as they allow for longitudinal collection of biofluids in which candidate biomarkers can be assessed. Given that endogenous microRNAs can be detected in the CSF (*36*), we hypothesized that our therapeutic microRNA mi*HTT* would also be present in CSF after intracranial rAAV5-miHTT administration. Indeed, whereas miHTT was undetectable in CSF pre-dose, CSF mi*HTT* concentrations were detected from the first time point studied (3 months post-injection), with sustained concentrations up to 12 months post-injection (**Figure 5A**).

Having shown that the active therapeutic molecule can be readily detectable in CSF indicating long-term durability of rAAV5-miHTT expression, we moved on to assess candidate HD biomarkers in CSF. Two of the most studied biofluid biomarkers to follow disease progression and therapeutic efficacy in HD are mHTT protein and NFL (*37*). As such, expression of both mHTT protein and NF-L was assessed in tgHD minipigs before treatment and at different timepoints after rAAV5-miHTT administration.

mHTT lowering in the striatum is partially reflected by mHTT lowering in CSF

First, we assessed mHTT protein in the CSF of control (naïve) tgHD animals. A longitudinal age-dependent increase in CSF mtHTT protein concentrations was observed (**Figure 5B**), which was confirmed by analysis of additional CSF samples from a previous study in older tgHD minipigs (*23*) (**Fig. S5A**). The 2B7-MW1 Singulex assay used for mHTT protein quantification is known to be dependent on (i) polyQ length (the longer the polyQ stretch, the higher the signal) and (ii) mHTT protein fragment length (the shorter the fragment, the higher the signal) (*34, 35*). The observed age-dependent increase could not be attributed to an increase in polyQ repeat with age of these animals, as somatic CAG repeat instability does not occur in this model given the presence of CAA interruptions in the DNA sequence (*27*). To exclude that the age-dependent increase in mHTT was due to mHTT protein fragmentation, samples were run with an alternative assay (2B7-2166, total HTT assay) which shows neither polyQ nor fragment dependency. Although this is a less sensitive assay, a good correlation between both assays was obtained (**Fig. S5B**), suggesting that the increase in mtHTT protein concentration with age in tgHD minipigs is a

concentration-dependent effect, and not due to any assay-related issues secondary to differences in polyQ length or fragment size.

Similar to control (naïve) tgHD animals, rAAV5-miHTT animals demonstrated an age-dependent increase in CSF mHTT concentration (**Figure 5B**). However, a significant treatment effect on CSF mHTT was observed over time and mHTT levels in rAAV5-miHTT animals were lower than in age-matched naïve controls, from 3 months post-treatment ($p<0.05$) (see **Table S1** for details on the statistical analysis). When compared to non-treated controls, CSF mHTT protein concentration was lower at 6- (27% lowering, 95%CI [3-51]) and 12-months (22% lowering, 95%CI [-5-49]) post-treatment (**Figure 5C**).

Transient increase CSF NFL after rAAV5-miHTT which normalizes by 3 months post-injection

Having determined mHTT lowering in CSF after one-time intracranial administration of rAAV5-miHTT, we analyzed NF-L as an additional biomarker which is linked both to efficacy and safety. There were no differences in NFL expression between wild-type and tgHD minipigs at 6 months of age, nor in a separate cohort of animals of increasing ages (up to 4 years old) (**Fig. S6**). Although this precluded us from assessing phenotypic improvement caused by rAAV5-miHTT, it still allowed us to assess the response of NFL to the administration procedure (**Figure 5D-E**). Following surgery, CSF NFL transiently increased (14- and 28-days post-injection) ($p<0.0001$). CSF NFL concentration in rAAV5-miHTT animals declined from 3 months onward ($p<0.001$), being comparable to those of naïve tgHD controls from 6 months on.

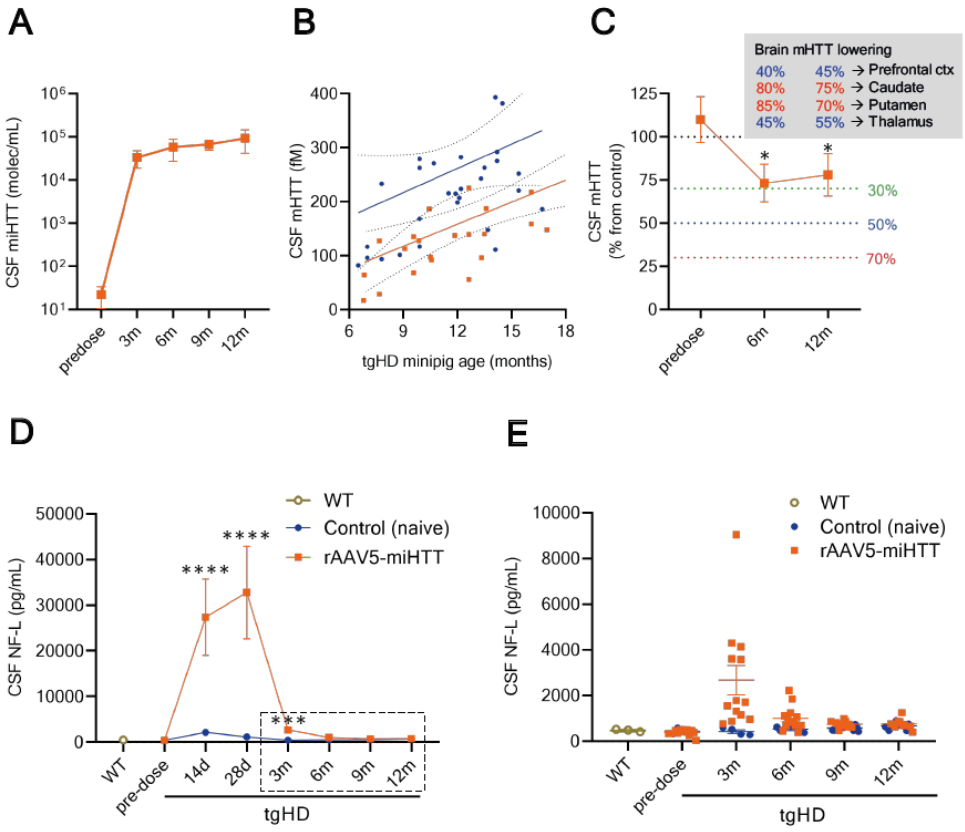

Figure 5. Biomarker measures in CSF of tgHD minipigs. (A) Therapeutic transgene miHTT concentration in CSF of rAAV5-miHTT injected animals (orange squares, representing average ± SEM) from 3 up to 12 months post-injection. **(B)** mHTT protein in CSF from control (blue dots) and rAAV5-miHTT (orange squares) tgHD minipigs according to age (in months); each point represents an individual measurement per animal; only data points from 3-months post-injection are displayed. Solid lines represent the best-fit line (linear regression), with their corresponding 95% confidence intervals indicated (dotted curves). **(C)** CSF mHTT protein lowering in rAAV5-miHTT animals expressed as percentage from age-matched controls; overlaying the graph, the panel indicates percentage lowering in different brain regions. *p<0.05. **(D)** CSF NF-L (as average ± SEM) over time following rAAV5-miHTT injection; dotted square indicates data zoomed-in in **(E)**, with individual CSF NF-L values at pre-dose and from 3 months post-injection. *Statistics: two-tailed t-test, corrected p ***<0.0005, ****<0.0001.*

Discussion

The therapeutic potential of rAAV5-miHTT has been demonstrated in different HD rodent models (*21, 22, 24*). To support successful transition of CNS gene therapies into the clinic, studies in large animal models are of high importance (*15, 23*). Critical issues for clinical translation include clinically feasible and precise delivery to target regions, potential of treatment efficacy in a larger brain, and availability of biomarkers for early prediction of therapeutic outcome. One of the key questions that is relevant for all HTT silencing therapies, is whether the striatum and cortex, the main areas affected in the disease, are effectively targeted in a large brain. We now show the feasibility and efficacy of MRI-guided CED for intracranial rAAV5-miHTT administration, resulting in coverage of relevant brain regions, long-term and well tolerated expression and target engagement. In addition, we evaluated the response of relevant candidate biomarkers in CSF to the therapeutic intervention.

In HD, neuropathology is not restricted to caudate and putamen as the initially affected regions, but extends to other areas with disease progression (*2*), especially cortical regions. Therapeutic coverage of all affected brain regions is considered essential. Targeted administration using CED has been shown to enhance the distribution of therapeutics in the brain parenchyma (*38*), also in pigs (*39*). Our first study in tgHD minipigs compared different surgical target regions (putamen, thalamus) to evaluate short-term efficacy of rAAV5-miHTT (*23*). Here we showed a detailed view of the dimensions of rAAV5-miHTT spread in a large brain, with substantial transduction in virtually all regions examined, except for brainstem and cerebellum, two regions that are not largely affected in HD (*2*). Our data suggest that thalamic injection might not be needed to achieve cortical coverage, which would avoid risks of direct injection in a sensitive relay station. The occurrence of thalamic calcification following complete HTT ablation (*40*), also suggests that thalamic administration should preferentially be avoided.

AAV-based gene therapies administered locally in specific brain regions extend to other brain regions based on transport of the virus though neuronal tracts. This is highly dependent on factors such as (i) surgical target region and (ii) AAV serotype (*41*). The present study supports the use of AAV5, based on its ability for retrograde and anterograde transport (*41, 42*), as vector for CNS disorders where a relatively wide coverage is needed. When compared to other AAV serotypes, AAV5 transduces neuronal populations at much greater efficiency (*43*), and shows the highest cortical spread in non-human primates (NHPs) (*44-46*), and mice (*47, 48*). One of the contributing factors leading to a greater spread of AAV5 and other serotypes (such as AAV1, AAV8 and AAV9), in contrast to AAV2 and AAV6, is the lack of heparin sulfate proteoglycan binding or binding to other AAV entry factors such as GPR108 (*49, 50*). In addition, AAV5 transduces both neurons and astrocytes (*13, 51*),

which has recently been shown to be required for phenotypic rescue in HD mice (*16*), in line with neurons and astrocytes being implicated in HD pathology (*52*).

Consistent with the broad pattern of transduction, we observed broad transgene expression and mHTT protein lowering, independently of regional differences in mHTT concentration, not only in the areas that showed substantial transduction, but also in areas with low concentrations of vector DNA. One hypothesis is that miHTT could be sorted into extracellular vesicles (EVs), leading to further spread of the active therapeutic molecule to neighboring cells, independently of neuronal connections. This is a plausible possibility given that miHTT is enclosed into the miR-451 backbone, and miR-451 has been shown to be enriched in EVs (*53, 54*). The combined effects of viral vector chosen, engineered miRNA design and potential contribution of EV-mediated spread of miHTT, are believed to contribute to the robust and sustained mHTT protein lowering by rAAV5-miHTT. Several other artificial miRNAs targeting human mHTT have been reported, but only few of those have been tested in large animal models (*55*). One of these, engineered into the miR-155 backbone and delivered via AAV9 (*18*) has been tested in HD sheep and showed a local transduction pattern (*56, 57*). Similar results were reported for other microRNA-based approaches in NHPs (*55, 58, 59*), delivered via AAV1 and AAV2, with effects restricted to striatum. Following intrathecal administration in NHP, HTT-targeting ASOs show an opposite pattern of HTT lowering, with predominant effects in cortex and spinal cord (*8*) and less anticipated lowering in deep brain regions (such as the caudate and putamen) affected earlier in HD (*7*).

An important aspect of gene therapies is the durability of expression, and in the CNS, long-lasting effects are expected. Indeed, we observed a similar degree of (ongoing) expression at 6- and 12-months post-administration, in line with rodent data (*22, 60, 61*). Striatal administration of AAV2 resulted in at least 8 years of transgene persistence in NHPs (*62*) and over 4 years in humans (*63*). As many aspects can influence long-term transgene expression (for example, DNA construct, promoter), we will continue to monitor animals remaining in the current study cohort. This will also allow us to assess potential phenotypic improvement in tgHD minipigs, with a disease phenotype expected to manifest at 4.5-6 years of age (*32*).

Early efficacy measures that allow prediction of beneficial therapeutic responses are much needed in slow progressive neurodegenerative diseases (*33, 37*). In HD, mHTT and NFL in CSF hold most promise to follow up disease progression and predict therapeutic response (*33, 37*). CSF mHTT expression in tgHD minipigs increased with age, which could not be attributed to technical issues, nor to somatic instability, absent in this model (*27*). The rapid rate of increase of CSF mHTT at this young age was unexpected, and may be attributed to neurodevelopment, although more data would be needed to support this

view. So far, this strong age effect has not been described in patients with HD (*35, 37, 64*), although longitudinal studies are still ongoing (hdclarity.net, *37*). We found a 25-30% lowering of mHTT protein in CSF of tgHD minipigs after treatment with rAAV5-miHTT, durable up to 1-year post administration. Hence, when compared to the 70-85% lowering observed the striatum, and the 40-45% lowering in the cortex, CSF mHTT concentrations underestimate parenchymal silencing induced by rAAV5-miHTT. The origin of CSF mHTT is still largely unknown, although preclinical studies suggest about 60% to be originating from CNS sources (*64*). However, the specific contributions of superficial (cortical) versus deep (striatum, thalamus) brain regions, and of tissues close to CSF collection (such as the lumbar spinal cord) are still to be elucidated. Because of this, although CSF mHTT concentrations have been proposed as a pharmacodynamic marker for ASO therapies (*7, 8*), its value for mHTT-silencing gene therapies remains to be determined, as well as its correlation (or lack thereof) with potential therapeutic effects. The present data in tgHD minipigs indicate that CSF mHTT concentrations underestimate the magnitude of parenchymal mHTT silencing induced by rAAV5-miHTT, urging the need of additional biomarkers for gene-therapy based HTT-lowering approaches.

NFL concentrations increase in the CSF of patients with neurodegenerative diseases, including HD (*35, 65*). Elevated NFL concentrations in the CSF and plasma of HD mutation carriers correlate with disease severity and with different measures of disease progression (*66*). Although NFL is used as a treatment response marker in other neurological diseases (*67-70*), no treatment response of NFL to potential disease-modifying drugs in HD has been evaluated preclinically, nor has it been observed in clinical trials so far (*7*). Recent clinical trials have reported a prolonged and dose-dependent elevation of NFL after intrathecal ASO administration (*7*), especially with high frequency of administration, and to a much lesser extent with longer intervals between dosing (*71*). In fact, the lack of HD-like phenotype in young tgHD minipigs in the current study precluded the evaluation of CSF NFL as a treatment response marker. The transient elevation of CSF NFL observed after injection was expected and can be attributed to the neurosurgery itself and local viral load as we have previously observed transient elevations in CSF cytokines after AAV5 brain administration in tgHD minipigs (*23*). Following the procedure NFL concentrations returned to baseline between 3- and 6-months post-surgery and did not increase during the rest of the study period. This is a similar profile to the CSF NFL profile observed in humans after deep brain stimulation (*72*). Hence, neither the neurosurgical approach, the exposure of the brain to rAAV5, the expression of the therapeutic miRNA nor the silencing of mutant huntingtin induced a long-term increase of NFL.

The pharmacokinetics of AAV-delivered miRNA-based therapies pose important challenges. As a specific pharmacokinetic marker of rAAV5-miHTT expression, we assessed the presence and persistence of mature miHTT in CSF of tgHD minipigs at different time

points after striatal administration. Our data indicate that it is possible to reliably detect miHTT in CSF from 3 up to 12 months post-injection, making this a suitable pharmacokinetic marker, and a true translational measure of long-term durability of rAAV5-miHTT.

The major limitation of this study is the use of untreated animals as controls, instead of a sham treatment group. This additional control would have been helpful in interpreting the results related to surgery itself, independently of the therapeutic construct, especially concerning disease CSF biomarkers (mHTT and NFL) which have been shown to respond to surgical trauma (*23, 72*). Group comparisons (rather than longitudinal analyses) were needed because the unexpectedly rapid rise in CSF mHTT, but would have been ideally done with respect animals receiving surgery, and this data should therefore be interpreted with caution. The results of NFL indicate that this would have been of more relevance shortly after surgery, and less from 3-6 months post-surgery. Other limitations are the use of young animals, and lack of disease-related phenotype at this age, making the bridging difficult between animal model and patients with manifest HD, currently the main target population of HTT lowering trials. Also, whether the same distribution would occur in adult animals, would need to be established. An additional limitation is the use of a single high dose for treatment, instead of different doses (low, mid, high). The dose used in the present study, causing profound (80-90%) mHTT lowering in target regions, is not the targeted translatable dose for the clinic. Considering the non-allele-selectivity of the approach, a target lowering of 50% would be considered adequate to avoid potential harmful effects of lowering wild type HTT as complete suppression of HTT may not be desirable because of its vital cellular functions (reviewed in *73*). As shown previously (*23*), the target porcine HTT sequence has two mismatches with miHTT, and therefore this tgHD model is not adequate to assess long-term HTT lowering tolerability. A final limitation is the lack of cell-specific analyses in tissue. Use of laser capture methods to determine the effects in different cell types, would be of added value, and can be considered for future studies.

Altogether, the results of this ongoing study indicate that intrastriatal CED delivery of rAAV5-miHTT results in pronounced, widespread and persistent silencing of mHTT in all brain areas that are known to be affected in HD. CSF mHTT concentrations underestimated silencing in the relevant deep brain areas and the current data do not support their use as a reliable biomarker for therapeutic efficacy, at least for intrastriatal gene therapy approaches. In contrast, mature CSF miHTT concentrations can be used as pharmacokinetic measure to monitor the expression and durability of rAAV5-miHTT delivery to the brain. These data, together with separate large animal GLP toxicology studies, support the further clinical development of the rAAV5-miHTT program into the clinic and shed light into the value of candidate biomarkers to follow-up efficacy.

Materials and Methods

Study design

The general study design is shown in **Table S2**. A total of n=31 animals were used in the study, with males and females equally distributed between groups. No sample size calculation was performed. Controls (naïve control group) did not receive any surgery or treatment (n=15). The treatment group (rAAV5-miHTT treated) received MRI-guided CED of rAAV5-miHTT (n=16). Animals were randomly distributed between control and treatment groups; rAAV5-miHTT treatment was administered without blinding. Control and treatment groups were randomly subdivided for interim sacrifices at 6 months (n=3-4 animals/group), 12 months (n=4 animals per group) or beyond 24 months post-surgery (n=8 animals/group). The present study presents data obtained up to 12 months post-surgery (animals beyond 24 months are still in in-life phase).

Animals

All components of this study were carried out in accordance with the Institutional Animal Care and Use Committee of Institute of Animal Physiology and Genetics, v.v.i. according to current Czech regulations. Male and female Libechov tgHD Göttingen minipigs (*27*) (n=31), ranging between 4-8 months of age at the beginning of the study, were used. The animals were screened for serum total and neutralizing rAAV5-antibodies before the start of the study, as previously described (*74*), selecting only animals considered seronegative (neutralizing antibody titers lower than 1:50 at baseline). Animals were housed under standard conditions of light and temperature (20 °C), with ad libitum access to food and water, and monitored daily for their general health status.

Vector design and production

cDNA encoding the miHTT cassette was packaged into rAAV5 by a baculovirus-based rAAV production system (uniQure) as described earlier (*75, 76*). The design and characterization of rAAV5-miHTT has been described previously (*20*). The complete transcription unit was flanked by two non-coding AAV-derived inverted terminal repeats, and expression was driven by a combination of the cytomegalovirus early enhancer element and chicken β-actin promoter (CAG promoter). The expression cassettes were inserted in a recombinant baculovirus vector by homologous recombination and clones were selected by plaque purification. The recombinant baculovirus containing the cassettes were further amplified and clones screened for best production and stability by PCR and qPCR. To generate AAV5, baculovirus infections on insect cells with recombinant baculoviruses was performed encoding rep for replication and packaging, cap-5 for the AAV5 capsid and the expression cassette. After viral particle assembled, prep purification was performed with AVB Sepharose high-performance affinity medium (GE Healthcare) using AKTA Explorer

purification system (GE Healthcare) and titer was determined by qPCR with specific primer-probe combinations against the CAG promoter.

MRI-guided delivery of rAAV5-miHTT

Pre-scan, surgery and MRI-guided CED drug delivery was performed using Renishaw pre-clinical drug delivery system. Briefly, animals were appropriately anesthetized as previously described (*23*) and placed in prone position in the MRI-compatible minipig fixation frame (Renishaw). After ensuring function of health monitoring systems the animal was placed into the MRI scanner. Prior to scanning, a fiducial arc (Renishaw) was attached to the frame. T1-weighted anatomical scan(s) with sufficient anatomical resolution were carried out with a cardio-coil in a 1.5 Tesla MRI. After finalizing scan(s), animals were transferred to the surgery room for cannula implantation.

Before surgery, the fiducial arc was removed from the fixation frame was replaced by a stereotactic frame. Using the precise coordinates from the prescan MRI, one burr hole per catheter was drilled. A total of 4 catheters were implanted bilaterally using a frontal approach, two catheters targeting the caudate nuclei and putamen on either side of the brain. After implantation, the frame was removed from the fixation frame and the animal transferred to the MRI for CED of 3 x 10^{13} vector genomes (vg)/mL (final dose of 1.2 x 10^{13} vg/brain) of rAAV5-miHTT mixed with a contrast agent (ProHance 2 mM, 1:500) (Bracco International B.V.). Infusions were carried out simultaneously over approximately 30 minutes with a starting infusion rate of 1 µL/min gradually increasing to a maximum rate of 3 µL/min. Real-time MRI scans were performed repeatedly during infusion and infusion rates were changed if there was any infusion flowback. The infusion was stopped when the target volume of 100 µL per in each of the four target brain areas was achieved. A final MRI scan was performed to document the filling of the target area. After infusion the guides and cannulas were carefully removed, the wound was closed up and the animal was allowed to recover in a warmed environment.

Blood and CSF sampling

Blood samples were collected from the ear vein, both for hematology (EDTA) and clinical blood chemistry (heparin) and processed, accordingly. To obtain plasma, the blood was centrifuged twice 10 min at 1500 G at 4°C, aliquoted and stored at -80°C.

CSF samples of approximately 3 mL were taken via lumbar puncture, under anesthesia (intramuscular TKX mixture: Tiletamin 4 mg/kg, Zolazepam 4 mg/kg, Ketamin 5 mg/kg and Xylazin 1 mg/kg; 1ml TKX mixture per 10-15kg body weight). All CSF processing was done on ice, within 15 minutes of collection. CSF was centrifuged at 2000 × g for 10 min at 4°C to remove cells and preserve cell integrity, supernatant was aliquoted in polypropylene tubes, snap-frozen and stored at -80°C.

Necropsy and brain tissue dissection

Euthanasia was performed using pentobarbital sodium intravenous injection, 100 mg/kg and followed by a bilateral thoracotomy. Animals were transcardially perfused with 500-1000 mL of heparinized PBS. The entire brain was carefully removed from the skull, placed into a brain matrix and coronally sliced into 3-4 mm blocks. The blocks were organized sequentially and identified with roman numbers as depicted in **Fig. S2**. In brains from the 6 months interim sacrifice, approximately n=54 brain punches of 4 mm in diameter from the uneven numbered slices were taken and individually stored in cryovials at -80°C until further use. Before biomolecular analysis, tissue punches from a single hemisphere (n=27 punches/animal) were cut into small pieces on dry ice, mixed, divided into four aliquots and stored at -80°C for subsequent use. In brains from the 12 months interim sacrifice, approximately n=170 brain punches of 4 mm in diameter were collected from all slices. The punches from a single hemisphere (n=85 punches/animal) were directly cut into small pieces, mixed, divided into four aliquots and stored at -80°C for subsequent use.

DNA isolation and determination of vector genome copies

For DNA isolation, one brain punch aliquot was used with the DNeasy 96 Blood and Tissue kit (Qiagen), following the manufacturer's instructions. Primers and probe specific for the polyA tail of the rAAV5-miHTT vector were used to amplify a specific target region of the vector with Taqman QPCR. The amount of vector DNA was calculated from a plasmid standard curve, which was taken along on the same plate. Results were reported as VG copies per µg of genomic DNA.

RNA isolation and determination of miHTT expression in brain tissue

For RNA isolation, one brain punch aliquot was homogenized in TRIzol reagent (Ambion, 15596018, ThermoFisher Scientific) and homogenized using Fast-Prep-24TM 5G (MP Biomedicals). Total RNA was isolated according to manufacturer's protocol (Direct-zol RNA MiniPrep kit, Zymo Research, R2052). To examine miHTT miRNA expression, cDNA was synthesized from isolated total RNA with custom made gene-specific RT primers targeting mature miHTT-24nt using TaqMan MicroRNA Reverse Transcription Kit (Applied Biosystems, ThermoFisher Scientific). A single stranded 24nt-long mature miHTT RNA standard line was taken along. Next, gene-specific TaqMan qPCR was performed with mature miHTT-24nt specific primers and probe using TaqMan Fast Universal PCR Master Mix (Applied Biosystems, ThermoFisher Scientific). Using the mature miHTT-24nt standard line, miHTT molecules per reaction were determined, and the number of miHTT-24nt molecules per cell subsequently calculated.

RNA isolation and determination of miHTT expression in CSF

RNA was isolated from a total of 300 µL minipig CSF using the miRNeasy Serum/Plasma Advanced Kit following manufacturer's protocol (Qiagen). During RNA isolation miR39 spike-in was added at step 4 (simultaneously with RPP buffer) at a concentration of 1.6x10^8 copies/µL as RNA isolation control. RNA samples were treated with dsDNAse (included in Maxima First Strand cDNA synthesis kit, Thermo Scientific, K1672) immediately after isolation.

To measure miRNA expression, RNA samples were retrotranscribed to cDNA with miRNA LNA RT kit and RT-qPCR was performed using miRCURY LNA miRNA PCR Assay kit (Qiagen), cel-miR-39-3p (YP00203952, Qiagen) and custom probes for detection of miHTT. miRNA expression levels were calculated as miHTT molecules/mL CSF based on a standard line performed with synthetic RNA oligos (Integrated DNA Technologies).

Mutant huntingtin (mHTT) protein quantification in brain tissue and CSF

Mutant huntingtin protein quantification in CSF and brain tissue samples was done using an ultrasensitive single molecule counting (SMC) immunossay (Singulex), as described previously (*34*). Briefly, pulverized tgHD minipig brain samples were homogenized in 170 µl ice cold lysis buffer using a FastPrep-96 tissue homogenizer and stored at -80°C until further testing. Homogenized brain samples or CSF (undiluted) were tested in technical triplicates. All CSF samples were tested for potential blood contamination using a species-independent colorimetric detection kit (Arbor) and following the manufacturer's instructions. Samples above the Hb threshold determined to interfere with the assay, were excluded from subsequent analyses. Final concentration of 15.6 fM to 3800 fM human HTT-Q46, 1-548 was used for quantification. For mutant HTT, the antibodies 2B7 (Novartis) directed against the N-terminal 7-13 amino acids of the huntingtin protein, and MW1 (Caltech) which binds to the expanded polyglutamine repeat, were used. For total HTT, a combination of 2B7 (Novartis) and MAB2166 (Sigma-Aldrich) were used. All analyses were performed at IRBM (Pomezia, Italy).

Neurofilament-light chain quantification in CSF

The UmanDiagnostics NF-light ELISA assay was used to quantify NFL concentrations in tgHD CSF, following the manufacturer's instructions (UmanDiagnostics). Different dilutions of CSF samples were used in order to ensure proper performance within the NFL standard curve. The obtained NF-L concentrations in CSF were expressed in pg/mL.

Statistics

Statistical analysis was performed in GraphPad Prism 8.0. Pearson correlation was used for correlation analyses. For comparison between two groups, two-tailed t-test

statistics were used, with multiple testing corrections. Regression analysis with graphical display of confidence intervals (95%CI) was used for the determination of the relationship between mHTT concentrations and age. Statistical analysis of mHTT in CSF was performed in SAS, using an analysis of covariance model (with treatment time, analysis batch and age as covariates). In all cases, the significance level was set to $p<0.05$.

Acknowledgments: We would like to thank Owen Lewis, Max Wooley and Dave Johnson from Renishaw, for their valuable support during the CED surgical procedure. The authors are grateful to the teams of Process Development and Analytical Development at uniQure for the production and characterization of rAAV5-miHTT, and to Eileen Sawyer and Ellen Broug for critically reading the manuscript. OCS Life Sciences provided support with statistical analysis of CSF mHTT. We are also grateful for the support from the CHDI Foundation, in particular Douglas MacDonald and David Howland.

Funding: Part of this work was supported by PIGMOD Center's sustainability program: National Sustainability Programme, project number LO1609 (Czech Ministry of Education, Youth and Sports) to JM.

Author contributions: Conceptualization: AV, MME, BBl, JM, ZE, HP, SVD, PK; Surgery: BBo, RL, DU, ZS, MC, BBl, ZE, JM; Sample collection: AV, MSG, CB, LP, JK, BB, ZE; Molecular and data analyses: AV, MME, AS, MSG, CB, CVT, SAB, LP RP, VF, AB; Formal Analysis: AV, MME; Writing: AV; Funding Acquisition: ZE, JM, HP, SVD, PK; Supervision: AV, MME, ZE, JM, PK.

Competing interests: AV, MME, AS, MSG, CB, CVT, SAB, LP, HP, SVD and PK are employees and shareholders at uniQure; ZE, JM and PIGMOD have a collaborative agreement with uniQure. Filed patent applications pertaining to the results presented in this paper include the following: RNAi induced huntingtin gene suppression (WO2016/102664, resulting in at least US 10,174,321 , US 10,767,180 and EP 3237618B1), A companion diagnostic to monitor the effects of gene therapy (PCT/EP2019/081759), Method and means to deliver miRNA to target cells (PCT/EP2019/081822) and Targeting misspliced transcripts in genetic disorders (PCT/EP2020/075871); the latter three have not yet published.

Data and materials availability: All data associated with this study are available in the main text or the supplementary materials, and, if required, materials may be available subject to at least an MTA.

References

1. G. P. Bates, R. Dorsey, J. F. Gusella, M. R. Hayden, C. Kay, B. R. Leavitt, M. Nance, C. A. Ross, R. I. Scahill, R. Wetzel, E. J. Wild, S. J. Tabrizi, Huntington disease. *Nat Rev Dis Primers* **1**, 15005 (2015).
2. H. J. Waldvogel, E. H. Kim, L. J. Tippett, J. P. Vonsattel, R. L. Faull, The Neuropathology of Huntington's Disease. *Curr Top Behav Neurosci* **22**, 33-80 (2015).
3. K. J. Wyant, A. J. Ridder, P. Dayalu, Huntington's Disease-Update on Treatments. *Curr Neurol Neurosci Rep* **17**, 33 (2017).
4. C. A. Ross, E. H. Aylward, E. J. Wild, D. R. Langbehn, J. D. Long, J. H. Warner, R. I. Scahill, B. R. Leavitt, J. C. Stout, J. S. Paulsen, R. Reilmann, P. G. Unschuld, A. Wexler, R. L. Margolis, S. J. Tabrizi, Huntington disease: natural history, biomarkers and prospects for therapeutics. *Nat Rev Neurol* **10**, 204-216 (2014).
5. S. J. Tabrizi, R. Ghosh, B. R. Leavitt, Huntingtin Lowering Strategies for Disease Modification in Huntington's Disease. *Neuron* **102**, 899 (2019).
6. P. McColgan, S. J. Tabrizi, Huntington's disease: a clinical review. *Eur J Neurol* **25**, 24-34 (2018).
7. S. J. Tabrizi, B. R. Leavitt, G. B. Landwehrmeyer, E. J. Wild, C. Saft, R. A. Barker, N. F. Blair, D. Craufurd, J. Priller, H. Rickards, A. Rosser, H. B. Kordasiewicz, C. Czech, E. E. Swayze, D. A. Norris, T. Baumann, I. Gerlach, S. A. Schobel, E. Paz, A. V. Smith, C. F. Bennett, R. M. Lane, I.-H. S. S. T. Phase 1-2a, Targeting Huntingtin Expression in Patients with Huntington's Disease. *N Engl J Med* **380**, 2307-2316 (2019).
8. H. B. Kordasiewicz, L. M. Stanek, E. V. Wancewicz, C. Mazur, M. M. McAlonis, K. A. Pytel, J. W. Artates, A. Weiss, S. H. Cheng, L. S. Shihabuddin, G. Hung, C. F. Bennett, D. W. Cleveland, Sustained therapeutic reversal of Huntington's disease by transient repression of huntingtin synthesis. *Neuron* **74**, 1031-1044 (2012).
9. J. F. Alterman, B. Godinho, M. R. Hassler, C. M. Ferguson, D. Echeverria, E. Sapp, R. A. Haraszti, A. H. Coles, F. Conroy, R. Miller, L. Roux, P. Yan, E. G. Knox, A. A. Turanov, R. M. King, G. Gernoux, C. Mueller, H. L. Gray-Edwards, R. P. Moser, N. C. Bishop, S. M. Jaber, M. J. Gounis, M. Sena-Esteves, A. A. Pai, M. DiFiglia, N. Aronin, A. Khvorova, A divalent siRNA chemical scaffold for potent and sustained modulation of gene expression throughout the central nervous system. *Nat Biotechnol* **37**, 884-894 (2019).
10. S. R. Choudhury, E. Hudry, C. A. Maguire, M. Sena-Esteves, X. O. Breakefield, P. Grandi, Viral vectors for therapy of neurologic diseases. *Neuropharmacology* **120**, 63-80 (2017).
11. S. Ingusci, G. Verlengia, M. Soukupova, S. Zucchini, M. Simonato, Gene Therapy Tools for Brain Diseases. *Front Pharmacol* **10**, 724 (2019).
12. Y. Chu, R. T. Bartus, F. P. Manfredsson, C. W. Olanow, J. H. Kordower, Long-term post-mortem studies following neurturin gene therapy in patients with advanced Parkinson's disease. *Brain* **143**, 960-975 (2020).
13. B. L. Davidson, C. S. Stein, J. A. Heth, I. Martins, R. M. Kotin, T. A. Derksen, J. Zabner, A. Ghodsi, J. A. Chiorini, Recombinant adeno-associated virus type 2, 4, and 5 vectors: transduction of variant cell types and regions in the mammalian central nervous system. *Proc Natl Acad Sci U S A* **97**, 3428-3432 (2000).
14. N. S. Caron, A. L. Southwell, C. C. Brouwers, L. D. Cengio, Y. Xie, H. F. Black, L. M. Anderson, S. Ko, X. Zhu, S. J. van Deventer, M. M. Evers, P. Konstantinova, M. R. Hayden, Potent and sustained huntingtin lowering via AAV5 encoding miRNA preserves striatal volume and cognitive function in a humanized mouse model of Huntington disease. *Nucleic Acids Res* **48**, 36-54 (2020).
15. J. Miniarikova, M. M. Evers, P. Konstantinova, Translation of MicroRNA-Based Huntingtin-Lowering Therapies from Preclinical Studies to the Clinic. *Mol Ther* **26**, 947-962 (2018).
16. L. M. Stanek, J. Bu, L. S. Shihabuddin, Astrocyte transduction is required for rescue of behavioral phenotypes in the YAC128 mouse model with AAV-RNAi mediated HTT lowering therapeutics. *Neurobiol Dis* **129**, 29-37 (2019).

17. L. M. Stanek, S. P. Sardi, B. Mastis, A. R. Richards, C. M. Treleaven, T. Taksir, K. Misra, S. H. Cheng, L. S. Shihabuddin, Silencing mutant huntingtin by adeno-associated virus-mediated RNA interference ameliorates disease manifestations in the YAC128 mouse model of Huntington's disease. *Hum Gene Ther* **25**, 461-474 (2014).
18. E. L. Pfister, K. O. Chase, H. Sun, L. A. Kennington, F. Conroy, E. Johnson, R. Miller, F. Borel, N. Aronin, C. Mueller, Safe and Efficient Silencing with a Pol II, but Not a Pol lII, Promoter Expressing an Artificial miRNA Targeting Human Huntingtin. *Mol Ther Nucleic Acids* **7**, 324-334 (2017).
19. B. Zeitler, S. Froelich, K. Marlen, D. A. Shivak, Q. Yu, D. Li, J. R. Pearl, J. C. Miller, L. Zhang, D. E. Paschon, S. J. Hinkley, I. Ankoudinova, S. Lam, D. Guschin, L. Kopan, J. M. Cherone, H. B. Nguyen, G. Qiao, Y. Ataei, M. C. Mendel, R. Amora, R. Surosky, J. Laganiere, B. J. Vu, A. Narayanan, Y. Sedaghat, K. Tillack, C. Thiede, A. Gartner, S. Kwak, J. Bard, L. Mrzljak, L. Park, T. Heikkinen, K. K. Lehtimaki, M. M. Svedberg, J. Haggkvist, L. Tari, M. Toth, A. Varrone, C. Halldin, A. E. Kudwa, S. Ramboz, M. Day, J. Kondapalli, D. J. Surmeier, F. D. Urnov, P. D. Gregory, E. J. Rebar, I. Munoz-Sanjuan, H. S. Zhang, Allele-selective transcriptional repression of mutant HTT for the treatment of Huntington's disease. *Nat Med* **25**, 1131-1142 (2019).
20. J. Miniarikova, I. Zanella, A. Huseinovic, T. van der Zon, E. Hanemaaijer, R. Martier, A. Koornneef, A. L. Southwell, M. R. Hayden, S. J. van Deventer, H. Petry, P. Konstantinova, Design, Characterization, and Lead Selection of Therapeutic miRNAs Targeting Huntingtin for Development of Gene Therapy for Huntington's Disease. *Mol Ther Nucleic Acids* **5**, e297 (2016).
21. J. Miniarikova, V. Zimmer, R. Martier, C. C. Brouwers, C. Pythoud, K. Richetin, M. Rey, J. Lubelski, M. M. Evers, S. J. van Deventer, H. Petry, N. Deglon, P. Konstantinova, AAV5-miHTT gene therapy demonstrates suppression of mutant huntingtin aggregation and neuronal dysfunction in a rat model of Huntington's disease. *Gene Ther* **24**, 630-639 (2017).
22. E. A. Spronck, C. C. Brouwers, A. Valles, M. de Haan, H. Petry, S. J. van Deventer, P. Konstantinova, M. M. Evers, AAV5-miHTT Gene Therapy Demonstrates Sustained Huntingtin Lowering and Functional Improvement in Huntington Disease Mouse Models. *Mol Ther Methods Clin Dev* **13**, 334-343 (2019).
23. M. M. Evers, J. Miniarikova, S. Juhas, A. Valles, B. Bohuslavova, J. Juhasova, H. K. Skalnikova, P. Vodicka, I. Valekova, C. Brouwers, B. Blits, J. Lubelski, H. Kovarova, Z. Ellederova, S. J. van Deventer, H. Petry, J. Motlik, P. Konstantinova, AAV5-miHTT Gene Therapy Demonstrates Broad Distribution and Strong Human Mutant Huntingtin Lowering in a Huntington's Disease Minipig Model. *Mol Ther* **26**, 2163-2177 (2018).
24. N. S. Caron, A. L. Southwell, C. C. Brouwers, L. D. Cengio, Y. Xie, H. F. Black, L. M. Anderson, S. Ko, X. Zhu, S. J. van Deventer, M. M. Evers, P. Konstantinova, M. R. Hayden, Potent and sustained huntingtin lowering via AAV5 encoding miRNA preserves striatal volume and cognitive function in a humanized mouse model of Huntington disease. *Nucleic Acids Res*, (2019).
25. S. Keskin, C. C. Brouwers, M. Sogorb-Gonzalez, R. Martier, J. A. Depla, A. Valles, S. J. van Deventer, P. Konstantinova, M. M. Evers, AAV5-miHTT Lowers Huntingtin mRNA and Protein without Off-Target Effects in Patient-Derived Neuronal Cultures and Astrocytes. *Mol Ther Methods Clin Dev* **15**, 275-284 (2019).
26. N. M. Lind, A. Moustgaard, J. Jelsing, G. Vajta, P. Cumming, A. K. Hansen, The use of pigs in neuroscience: modeling brain disorders. *Neurosci Biobehav Rev* **31**, 728-751 (2007).
27. M. Baxa, M. Hruska-Plochan, S. Juhas, P. Vodicka, A. Pavlok, J. Juhasova, A. Miyanohara, T. Nejime, J. Klima, M. Macakova, S. Marsala, A. Weiss, S. Kubickova, P. Musilova, R. Vrtel, E. M. Sontag, L. M. Thompson, J. Schier, H. Hansikova, D. S. Howland, E. Cattaneo, M. DiFiglia, M. Marsala, J. Motlik, A transgenic minipig model of Huntington's Disease. *J Huntingtons Dis* **2**, 47-68 (2013).
28. T. Ardan, M. Baxa, B. Levinska, M. Sedlackova, T. D. Nguyen, J. Klima, S. Juhas, J. Juhasova, P. Smatlikova, P. Vochozkova, J. Motlik, Z. Ellederova, Transgenic minipig model of Huntington's disease exhibiting gradually progressing neurodegeneration. *Dis Model Mech*, (2019).

29. J. Krizova, H. Stufkova, M. Rodinova, M. Macakova, B. Bohuslavova, D. Vidinska, J. Klima, Z. Ellederova, A. Pavlok, D. S. Howland, J. Zeman, J. Motlik, H. Hansikova, Mitochondrial Metabolism in a Large-Animal Model of Huntington Disease: The Hunt for Biomarkers in the Spermatozoa of Presymptomatic Minipigs. *Neurodegener Dis* **17**, 213-226 (2017).
30. M. Rodinova, J. Krizova, H. Stufkova, B. Bohuslavova, G. Askeland, Z. Dosoudilova, S. Juhas, J. Juhasova, Z. Ellederova, J. Zeman, L. Eide, J. Motlik, H. Hansikova, Deterioration of mitochondrial bioenergetics and ultrastructure impairment in skeletal muscle of a transgenic minipig model in the early stages of Huntington's disease. *Dis Model Mech* **12**, (2019).
31. D. Vidinska, P. Vochozkova, P. Smatlikova, T. Ardan, J. Klima, S. Juhas, J. Juhasova, B. Bohuslavova, M. Baxa, I. Valekova, J. Motlik, Z. Ellederova, Gradual Phenotype Development in Huntington Disease Transgenic Minipig Model at 24 Months of Age. *Neurodegener Dis* **18**, 107-119 (2018).
32. M. Baxa, B. Levinska, M. Skrivankova, M. Pokorny, J. Juhasova, J. Klima, J. Klempir, S. Juhas, Z. Ellederova, Longitudinal study revealed motor, cognitive and behavioral decline in transgenic minipig model of Huntington's disease. *Dis Model Mech*, (2019).
33. F. B. Rodrigues, L. M. Byrne, E. J. Wild, Biofluid Biomarkers in Huntington's Disease. *Methods Mol Biol* **1780**, 329-396 (2018).
34. V. Fodale, R. Boggio, M. Daldin, C. Cariulo, M. C. Spiezia, L. M. Byrne, B. R. Leavitt, E. J. Wild, D. Macdonald, A. Weiss, A. Bresciani, Validation of Ultrasensitive Mutant Huntingtin Detection in Human Cerebrospinal Fluid by Single Molecule Counting Immunoassay. *J Huntingtons Dis* **6**, 349-361 (2017).
35. E. J. Wild, R. Boggio, D. Langbehn, N. Robertson, S. Haider, J. R. Miller, H. Zetterberg, B. R. Leavitt, R. Kuhn, S. J. Tabrizi, D. Macdonald, A. Weiss, Quantification of mutant huntingtin protein in cerebrospinal fluid from Huntington's disease patients. *J Clin Invest* **125**, 1979-1986 (2015).
36. M. M. J. van den Berg, J. Krauskopf, J. G. Ramaekers, J. C. S. Kleinjans, J. Prickaerts, J. J. Briede, Circulating microRNAs as potential biomarkers for psychiatric and neurodegenerative disorders. *Prog Neurobiol*, 101732 (2019).
37. L. M. Byrne, F. B. Rodrigues, E. B. Johnson, P. A. Wijeratne, E. De Vita, D. C. Alexander, G. Palermo, C. Czech, S. Schobel, R. I. Scahill, A. Heslegrave, H. Zetterberg, E. J. Wild, Evaluation of mutant huntingtin and neurofilament proteins as potential markers in Huntington's disease. *Sci Transl Med* **10**, (2018).
38. R. H. Bobo, D. W. Laske, A. Akbasak, P. F. Morrison, R. L. Dedrick, E. H. Oldfield, Convection-enhanced delivery of macromolecules in the brain. *Proc Natl Acad Sci U S A* **91**, 2076-2080 (1994).
39. N. U. Barua, M. Woolley, A. S. Bienemann, D. Johnson, M. J. Wyatt, C. Irving, O. Lewis, E. Castrique, S. S. Gill, Convection-enhanced delivery of AAV2 in white matter--a novel method for gene delivery to cerebral cortex. *J Neurosci Methods* **220**, 1-8 (2013).
40. P. Dietrich, I. M. Johnson, S. Alli, I. Dragatsis, Elimination of huntingtin in the adult mouse leads to progressive behavioral deficits, bilateral thalamic calcification, and altered brain iron homeostasis. *PLoS Genet* **13**, e1006846 (2017).
41. L. Samaranch, B. Blits, W. San Sebastian, P. Hadaczek, J. Bringas, V. Sudhakar, M. Macayan, P. J. Pivirotto, H. Petry, K. S. Bankiewicz, MR-guided parenchymal delivery of adeno-associated viral vector serotype 5 in non-human primate brain. *Gene Ther* **24**, 253-261 (2017).
42. M. E. Emborg, S. A. Hurley, V. Joers, P. M. Tromp do, C. R. Swanson, S. Ohshima-Hosoyama, V. Bondarenko, K. Cummisford, M. Sonnemans, S. Hermening, B. Blits, A. L. Alexander, Titer and product affect the distribution of gene expression after intraputaminal convection-enhanced delivery. *Stereotact Funct Neurosurg* **92**, 182-194 (2014).
43. E. A. Markakis, K. P. Vives, J. Bober, S. Leichtle, C. Leranth, J. Beecham, J. D. Elsworth, R. H. Roth, R. J. Samulski, D. E. Redmond, Jr., Comparative transduction efficiency of AAV vector serotypes 1-6 in the substantia nigra and striatum of the primate brain. *Mol Ther* **18**, 588-593 (2010).
44. A. Gerits, P. Vancraeyenest, S. Vreysen, M. E. Laramee, A. Michiels, R. Gijsbers, C. Van den Haute, L. Moons, Z. Debyser, V. Baekelandt, L. Arckens, W. Vanduffel, Serotype-dependent transduction

efficiencies of recombinant adeno-associated viral vectors in monkey neocortex. *Neurophotonics* **2**, 031209 (2015).
45. I. Diester, M. T. Kaufman, M. Mogri, R. Pashaie, W. Goo, O. Yizhar, C. Ramakrishnan, K. Deisseroth, K. V. Shenoy, An optogenetic toolbox designed for primates. *Nat Neurosci* **14**, 387-397 (2011).
46. M. A. Colle, F. Piguet, L. Bertrand, S. Raoul, I. Bieche, L. Dubreil, D. Sloothaak, C. Bouquet, P. Moullier, P. Aubourg, Y. Cherel, N. Cartier, C. Sevin, Efficient intracerebral delivery of AAV5 vector encoding human ARSA in non-human primate. *Hum Mol Genet* **19**, 147-158 (2010).
47. J. M. Taymans, L. H. Vandenberghe, C. V. Haute, I. Thiry, C. M. Deroose, L. Mortelmans, J. M. Wilson, Z. Debyser, V. Baekelandt, Comparative analysis of adeno-associated viral vector serotypes 1, 2, 5, 7, and 8 in mouse brain. *Hum Gene Ther* **18**, 195-206 (2007).
48. I. Scheyltjens, M. E. Laramee, C. Van den Haute, R. Gijsbers, Z. Debyser, V. Baekelandt, S. Vreysen, L. Arckens, Evaluation of the expression pattern of rAAV2/1, 2/5, 2/7, 2/8, and 2/9 serotypes with different promoters in the mouse visual cortex. *J Comp Neurol* **523**, 2019-2042 (2015).
49. B. E. Deverman, B. M. Ravina, K. S. Bankiewicz, S. M. Paul, D. W. Y. Sah, Gene therapy for neurological disorders: progress and prospects. *Nat Rev Drug Discov* **17**, 641-659 (2018).
50. A. M. Dudek, N. Zabaleta, E. Zinn, S. Pillay, J. Zengel, C. Porter, J. S. Franceschini, R. Estelien, J. E. Carette, G. L. Zhou, L. H. Vandenberghe, GPR108 Is a Highly Conserved AAV Entry Factor. *Mol Ther* **28**, 367-381 (2020).
51. C. Burger, O. S. Gorbatyuk, M. J. Velardo, C. S. Peden, P. Williams, S. Zolotukhin, P. J. Reier, R. J. Mandel, N. Muzyczka, Recombinant AAV viral vectors pseudotyped with viral capsids from serotypes 1, 2, and 5 display differential efficiency and cell tropism after delivery to different regions of the central nervous system. *Mol Ther* **10**, 302-317 (2004).
52. M. Gray, Astrocytes in Huntington's Disease. *Adv Exp Med Biol* **1175**, 355-381 (2019).
53. J. Guduric-Fuchs, A. O'Connor, B. Camp, C. L. O'Neill, R. J. Medina, D. A. Simpson, Selective extracellular vesicle-mediated export of an overlapping set of microRNAs from multiple cell types. *BMC Genomics* **13**, 357 (2012).
54. R. Reshke, J. A. Taylor, A. Savard, H. Guo, L. H. Rhym, P. S. Kowalski, M. T. Trung, C. Campbell, W. Little, D. G. Anderson, D. Gibbings, Reduction of the therapeutic dose of silencing RNA by packaging it in extracellular vesicles via a pre-microRNA backbone. *Nat Biomed Eng* **4**, 52-68 (2020).
55. M. S. Keiser, H. B. Kordasiewicz, J. L. McBride, Gene suppression strategies for dominantly inherited neurodegenerative diseases: lessons from Huntington's disease and spinocerebellar ataxia. *Hum Mol Genet* **25**, R53-64 (2016).
56. E. L. Pfister, N. DiNardo, E. Mondo, F. Borel, F. Conroy, C. Fraser, G. Gernoux, X. Han, D. Hu, E. Johnson, L. Kennington, P. Liu, S. J. Reid, E. Sapp, P. Vodicka, T. Kuchel, A. J. Morton, D. Howland, R. Moser, M. Sena-Esteves, G. Gao, C. Mueller, M. DiFiglia, N. Aronin, Artificial miRNAs Reduce Human Mutant Huntingtin Throughout the Striatum in a Transgenic Sheep Model of Huntington's Disease. *Hum Gene Ther* **29**, 663-673 (2018).
57. J. C. Jacobsen, C. S. Bawden, S. R. Rudiger, C. J. McLaughlan, S. J. Reid, H. J. Waldvogel, M. E. MacDonald, J. F. Gusella, S. K. Walker, J. M. Kelly, G. C. Webb, R. L. Faull, M. I. Rees, R. G. Snell, An ovine transgenic Huntington's disease model. *Hum Mol Genet* **19**, 1873-1882 (2010).
58. J. L. McBride, M. R. Pitzer, R. L. Boudreau, B. Dufour, T. Hobbs, S. R. Ojeda, B. L. Davidson, Preclinical safety of RNAi-mediated HTT suppression in the rhesus macaque as a potential therapy for Huntington's disease. *Mol Ther* **19**, 2152-2162 (2011).
59. R. Grondin, M. D. Kaytor, Y. Ai, P. T. Nelson, D. R. Thakker, J. Heisel, M. R. Weatherspoon, J. L. Blum, E. N. Burright, Z. Zhang, W. F. Kaemmerer, Six-month partial suppression of Huntingtin is well tolerated in the adult rhesus striatum. *Brain* **135**, 1197-1209 (2012).
60. S. E. Leff, S. K. Spratt, R. O. Snyder, R. J. Mandel, Long-term restoration of striatal L-aromatic amino acid decarboxylase activity using recombinant adeno-associated viral vector gene transfer in a rodent model of Parkinson's disease. *Neuroscience* **92**, 185-196 (1999).

61. D. Sondhi, D. A. Peterson, E. L. Giannaris, C. T. Sanders, B. S. Mendez, B. De, A. B. Rostkowski, B. Blanchard, K. Bjugstad, J. R. Sladek, Jr., D. E. Redmond, Jr., P. L. Leopold, S. M. Kaminsky, N. R. Hackett, R. G. Crystal, AAV2-mediated CLN2 gene transfer to rodent and non-human primate brain results in long-term TPP-I expression compatible with therapy for LINCL. *Gene Ther* **12**, 1618-1632 (2005).
62. P. Hadaczek, J. L. Eberling, P. Pivirotto, J. Bringas, J. Forsayeth, K. S. Bankiewicz, Eight years of clinical improvement in MPTP-lesioned primates after gene therapy with AAV2-hAADC. *Mol Ther* **18**, 1458-1461 (2010).
63. G. Mittermeyer, C. W. Christine, K. H. Rosenbluth, S. L. Baker, P. Starr, P. Larson, P. L. Kaplan, J. Forsayeth, M. J. Aminoff, K. S. Bankiewicz, Long-term evaluation of a phase 1 study of AADC gene therapy for Parkinson's disease. *Hum Gene Ther* **23**, 377-381 (2012).
64. A. L. Southwell, S. E. Smith, T. R. Davis, N. S. Caron, E. B. Villanueva, Y. Xie, J. A. Collins, M. L. Ye, A. Sturrock, B. R. Leavitt, A. G. Schrum, M. R. Hayden, Ultrasensitive measurement of huntingtin protein in cerebrospinal fluid demonstrates increase with Huntington disease stage and decrease following brain huntingtin suppression. *Sci Rep* **5**, 12166 (2015).
65. R. Constantinescu, M. Romer, D. Oakes, L. Rosengren, K. Kieburtz, Levels of the light subunit of neurofilament triplet protein in cerebrospinal fluid in Huntington's disease. *Parkinsonism Relat Disord* **15**, 245-248 (2009).
66. L. M. Byrne, F. B. Rodrigues, K. Blennow, A. Durr, B. R. Leavitt, R. A. C. Roos, R. I. Scahill, S. J. Tabrizi, H. Zetterberg, D. Langbehn, E. J. Wild, Neurofilament light protein in blood as a potential biomarker of neurodegeneration in Huntington's disease: a retrospective cohort analysis. *Lancet Neurol* **16**, 601-609 (2017).
67. J. Kuhle, G. Disanto, J. Lorscheider, T. Stites, Y. Chen, F. Dahlke, G. Francis, A. Shrinivasan, E. W. Radue, G. Giovannoni, L. Kappos, Fingolimod and CSF neurofilament light chain levels in relapsing-remitting multiple sclerosis. *Neurology* **84**, 1639-1643 (2015).
68. A. Mellgren, R. W. Price, L. Hagberg, L. Rosengren, B. J. Brew, M. Gisslen, Antiretroviral treatment reduces increased CSF neurofilament protein (NFL) in HIV-1 infection. *Neurology* **69**, 1536-1541 (2007).
69. B. Olsson, L. Alberg, N. C. Cullen, E. Michael, L. Wahlgren, A. K. Kroksmark, K. Rostasy, K. Blennow, H. Zetterberg, M. Tulinius, NFL is a marker of treatment response in children with SMA treated with nusinersen. *J Neurol* **266**, 2129-2136 (2019).
70. J. Kuhle, H. Kropshofer, D. A. Haering, U. Kundu, R. Meinert, C. Barro, F. Dahlke, D. Tomic, D. Leppert, L. Kappos, Blood neurofilament light chain as a biomarker of MS disease activity and treatment response. *Neurology* **92**, e1007-e1015 (2019).
71. S. A. Schobel. (2020).
72. R. Constantinescu, B. Holmberg, L. Rosengren, O. Corneliusson, B. Johnels, H. Zetterberg, Light subunit of neurofilament triplet protein in the cerebrospinal fluid after subthalamic nucleus stimulation for Parkinson's disease. *Acta Neurol Scand* **124**, 206-210 (2011).
73. F. Saudou, S. Humbert, The Biology of Huntingtin. *Neuron* **89**, 910-926 (2016).
74. A. Majowicz, D. Salas, N. Zabaleta, E. Rodriguez-Garcia, G. Gonzalez-Aseguinolaza, H. Petry, V. Ferreira, Successful Repeated Hepatic Gene Delivery in Mice and Non-human Primates Achieved by Sequential Administration of AAV5(ch) and AAV1. *Mol Ther* **25**, 1831-1842 (2017).
75. M. Urabe, C. Ding, R. M. Kotin, Insect cells as a factory to produce adeno-associated virus type 2 vectors. *Hum Gene Ther* **13**, 1935-1943 (2002).
76. C. Unzu, S. Hervas-Stubbs, A. Sampedro, I. Mauleon, U. Mancheno, C. Alfaro, R. E. de Salamanca, A. Benito, S. G. Beattie, H. Petry, J. Prieto, I. Melero, A. Fontanellas, Transient and intensive pharmacological immunosuppression fails to improve AAV-based liver gene transfer in non-human primates. *J Transl Med* **10**, 122 (2012).

Supplementary Tables

Table S1. Statistical analysis of mHTT in CSF of tgHD minipigs (control versus treated).

Type 3 tests of fixed effects				
Effect	Num DF	Den DF	F Value	Pr > F
Treatment	1	28.8	5.64	0.0244
Time	3	44.9	0.79	0.5036
Analysis_batch	1	58.8	14.13	0.0004
Treatment*Time	4	47.9	0.32	0.8634
Contrasts				
Comparison	N	Confidence Interval	P	
Average effect over time	73	0.568 (0.412-0.784)	0.001	
Treatment versus control at T=6 months	73	0.668 (0.449-0.993)	0.046	
Treatment versus control at T=9 months	73	0.551 (0.378-0.803)	0.003	
Treatment versus control at T=12 months	73	0.657 (0.438-0.984)	0.042	

Analysis of covariance model: logAVG mHTT (fM)= Treatment Time Analysis_batch Treatment*Time Age_at_collection

NOTE: Raw estimates based on the log transformed AVG mHTT (fM) were back transformed, presenting the ratio of treatment versus control with 95% confidence intervals and p-values for the average effect over time and at each time point

Table S2. Study design of intrastriatal microRNA-based gene therapy in tgHD minipigs.

Timepoint	-7 d	0	7 d	14 d	28 d	3 mo	6 mo	9 mo	12 mo	15 mo	18 mo	21 mo	24 mo	>24 mo**
TgHD minipigs														
1. Naive 6mo (n = 3)							†							
2. Naive 12mo (n = 4)									†					
3. Naive >24mo (n = 8)														
4. rAAV5miHTT 6mo (n = 3*)							†							
5. rAAV5miHTT 12mo (n = 4)									†					
6. rAAV5miHTT >24mo (n = 8)														
MRI-guided CED (groups 4 to 6)		x												
Blood and CSF collection	x		x	x	x	x	x	x	x	x	x	x	x	
Sacrifice and brain collection							x		x					

: in life, †: sacrifice, **: phenotypic follow-up, d: days, mo: months

*Note: Initial group size was n=4, but one animal did not recover from anesthesia during CSF collection at 28d post-injection

Supplementary Figures

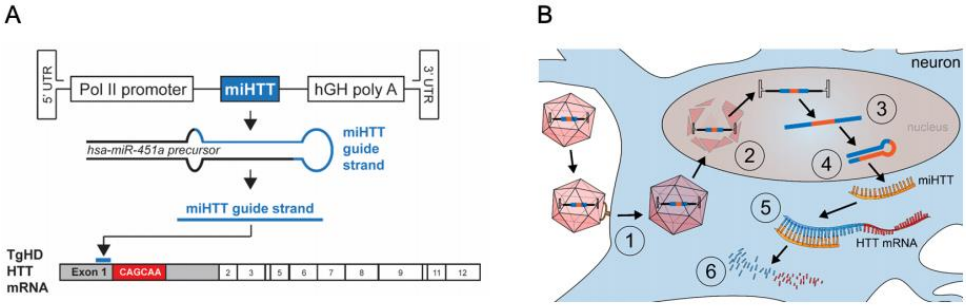

Fig. S1. **Design and mechanism of action of rAAV5-miHTT leading to HTT lowering in the cell. (A)** The DNA construct is comprised of miHTT, an artificial microRNA in which the guide strand of hs-miR-451a has been modified to specifically target human HTT; miHTT is flanked by a pol II promoter, and a hGH polyA signal at the 5' and 3' ends, respectively, as well as inverted terminal repeats (ITR) at each end. The miHTT guide strand binds 5' from the expanded CAG repeat, therefore targeting human HTT exon 1. In tgHD minipigs, the CAG expansion repeat is regularly interrupted with by CAA to avoid somatic instability in this model. **(B)** The mechanism of action can be described in several steps. (1) Upon parenchymal injection AAV5-miHTT binds to neuronal cell-surface receptors and is internalized. (2) Transport to the nucleus and uncoating of the miHTT transgene which remains mostly episomal. (3) Expression and processing of the miHTT transgene by the endogenous RNA interference machinery; (4) Hairpin structured precursor is transported to the cytoplasm and further processed to mature guide miHTT. No passenger strand is formed, strongly limiting the risk of off-target activity. (5) Mature miHTT is loaded in the RNA-induced silencing complex and binds HTT mRNA. (6) HTT mRNA is cleaved and degraded, resulting in lowering of HTT protein translation.

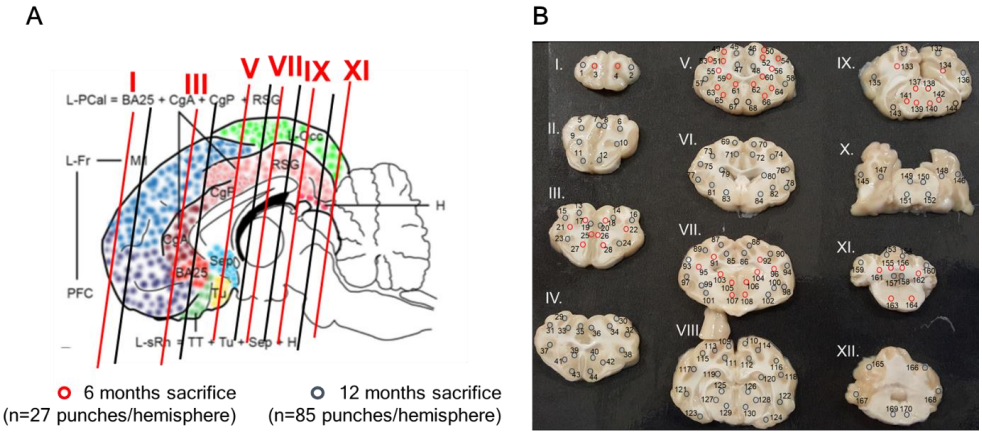

Fig. S2. Brain dissection scheme for bioanalytics. (A) tgHD minipig brains were cut in coronal sections of 4mm thick (12 sections in total, numbered in roman numbers I to XII). Brain regions of interest for bioanalyses were dissected by micropunch, using uneven sections (in the case of 6 months interim sacrifice) or both even and uneven (for 12 months interim sacrifice). **(B)** Scheme depicting the position of the punches (4 mm in diameter) to dissect brain regions of interest. In red, regions dissected for the 6-month interim sacrifice. In dark blue, additional regions dissected after the 12 months interim sacrifice.

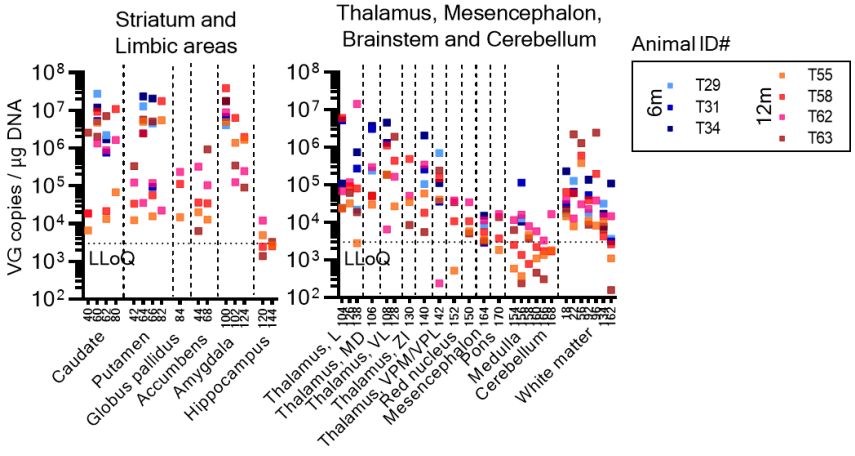

Fig. S3. Vector genome copies in deep brain regions of tgHD minipigs at 6- and 12-months post rAAV5-miHTT administration in caudate and putamen. Concentrations of vector DNA (expressed as vector genome copies/ µg genomic DNA) in striatum, limbic areas, thalamus, brainstem and cerebellum, are shown. In blue, animals sacrificed at 6 months (coded T29, T31 and T34). In shades of orange to pink, animals sacrificed at 12 months (coded T55, T58, T62 and T63). Each square represents an individual punch. VGconcentrations were above LLoQ in all brain regions, except partly in hippocampus, cerebellum, white matter and individual brainstem nuclei. *LLoQ: lower limit of quantification.*

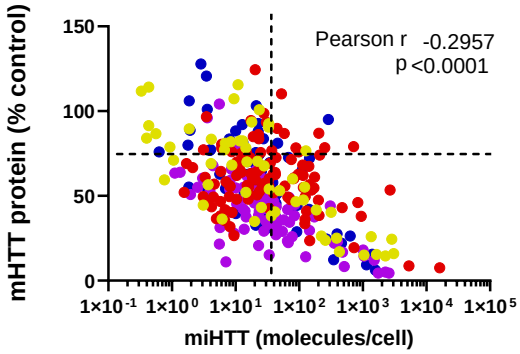

Fig. S4. Correlation between miHTT expression and mHTT protein lowering (as % from control), 12months post rAAV5-miHTT administration. Each color represents one of the 4 animals of the treated group, sacrificed at 12 months post-treatment.

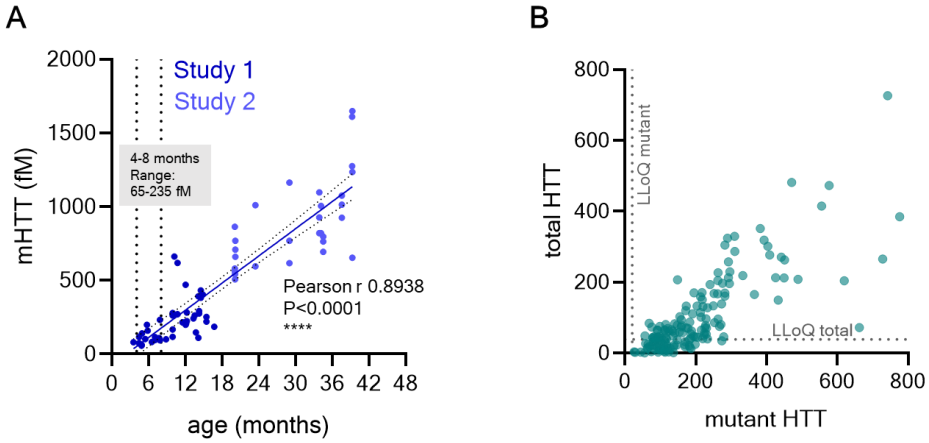

Fig. S5. Huntingtin protein concentrationsin CSF of tgHD minipigs increase with age, as determined by two independent immunoassays. (A) Mutant HTT (mHTT) protein concentrations in CSF (expressed in fM) using samples from two independent studies with untreated tgHD minipigs of different ages. **(B)** Quantification of total and mutant HTT using an independent immunoassay. *LLoQ: lower limit of quantification.*

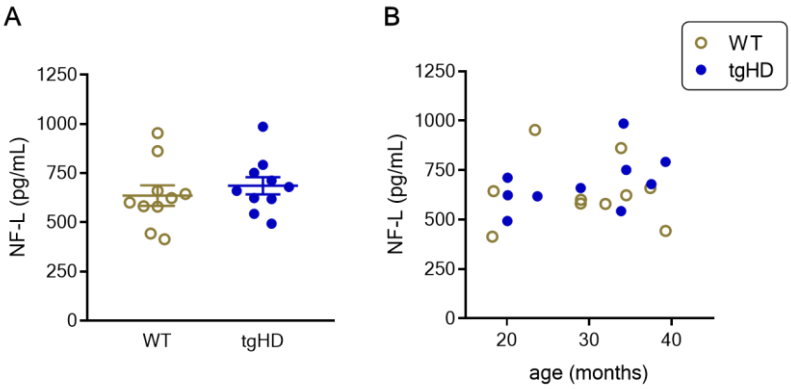

Fig. S6. No differences in CSF neurofilament light chain (NF-L) between wild type (WT) and transgenic HD minipigs (TG) up to 4 years of age. (A) NF-L concentrations in WT and tgHDminipigss and **(B)** CSF NF-L concentration by age in WT and tgHD minipigs.